LIMNOLOGY
and
OCEANOGRAPHY

ASLO

Limnol. Oceanogr. 60, 2015, 329–345
© 2015 Association for the Sciences of Limnology and Oceanography
doi: 10.1111/lno.10029

Dynamic hydrologic and biogeochemical processes drive microbially enhanced iron and sulfur cycling within the intertidal mixing zone of a beach aquifer

Sean M. McAllister,[1] Joshua M. Barnett,[2] James W. Heiss,[3] Alyssa J. Findlay,[1] Daniel J. MacDonald,[4] Charles L. Dow,[5] George W. Luther, III,[1,4] Holly A. Michael,[3,6] Clara S. Chan*[1,3]

[1]School of Marine Science and Policy, University of Delaware, Newark and Lewes, Delaware
[2]Department of Biological Sciences, University of Delaware, Newark, Delaware
[3]Department of Geological Sciences, University of Delaware, Newark, Delaware
[4]Department of Chemistry and Biochemistry, University of Delaware, Newark, Delaware
[5]Stroud Water Research Center, Avondale, Pennsylvania
[6]Department of Civil and Environmental Engineering, University of Delaware, Newark, Delaware

Abstract

Intertidal aquifers host a reactive zone comprised of Fe mineral-coated sands where fresh and saline groundwaters mix. This zone may significantly influence the export of C, N, P, Fe, and other metals in submarine groundwater discharge (SGD). Toward determining the roles of microbes in Fe and S mineralization, and the interplay of microbiology with geochemistry and physical hydrology, we conducted a biogeochemical study of pore waters at Cape Shores, Delaware. Here, fresh groundwater provides Fe(II), which precipitates as $Fe^{III}OOH$ predominantly through microbial Fe(II) oxidation. Candidate division OP3 was the dominant microbial group associated with Fe(II)- and Fe(III)-rich regions of the aquifer, suggesting that this uncharacterized phylum may be involved in Fe(II) oxidation. Saline water brings O_2, sulfate, and organic C into the intertidal mixing zone. Microbial reduction of sulfate produces sulfide that is transported to the Fe-mineralized zone leading to the transformation of FeOOH to Fe(II) sulfides. Microbial populations are structured by the availability of chemical species supplied along groundwater flow paths. Seasonal changes in the relative supply of fresh and saline groundwater affect solute fluxes, and therefore, microbial controls on the location and composition of the Fe-mineralized zone. Ultimately, the composition, extent, and dynamics of the Fe-mineralized zone will affect the sequestration, affinity, and residence time of solutes bound for export to coastal oceans through SGD.

Submarine groundwater discharge (SGD) contributes chemical loads comparable to those of rivers, affecting solute flux to coastal waters and ultimately the global oceans (Moore 2008). SGD-derived nutrients drastically affect coastal ecosystems through enhanced primary production, at times leading to wide-scale eutrophication and hypoxia. Discharged metals, such as the limiting micronutrient Fe, can lead to large scale blooms of microbial communities (Smetacek et al. 2012). The effect of these solute fluxes from groundwater has received increasing attention within the last decade (Moore 2010). However, less research has focused on the processes affecting the SGD-derived chemical load prior to discharge. Knowing these mechanisms is critical to understanding and predicting SGD geochemistry, and therefore, its effects on marine biogeochemical cycles (Martin 2009).

*Correspondence: cschan@udel.edu

The intertidal mixing zone of a beach aquifer can host many different biogeochemical reactions as fresh and saline groundwaters mix before exiting the aquifer as SGD (Fig. 1A). Freshwater discharge driven by the terrestrial hydraulic gradient (Fig. 1A, process 1) originates both inland and locally. Saltwater flow in the beach aquifer is driven by two primary mechanisms. Seawater infiltration along the upper intertidal zone due to tide and wave dynamics results in a shallow intertidal circulation cell (Fig. 1A, process 2; Michael et al. 2005; Robinson et al. 2006), and the density gradient along the lower freshwater-saltwater interface results in a larger deep circulation cell (Fig. 1A, process 3). The varying sources, residence times, and flow paths of groundwater in these three zones lead to differences in inputs of redox-active solutes, including organic C and N, O_2, and Fe and S species, resulting in reactions along mixing interfaces (Slomp and Van Cappellen 2004; Charette and Sholkovitz 2006).

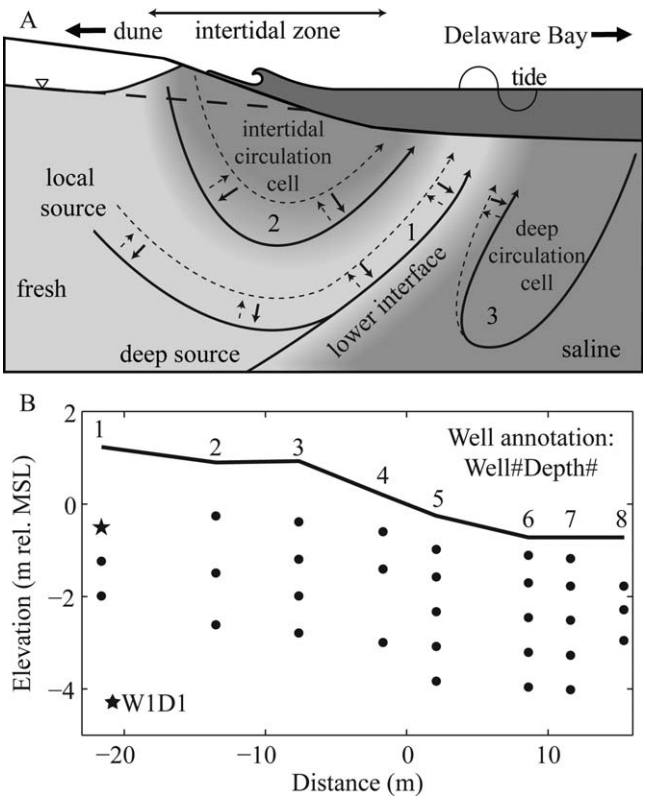

Fig. 1. (A) Diagram of the intertidal mixing zone at Cape Henlopen, showing three simplified flow paths discussed in the text. Decreased freshwater flux (feature 1) leads to a deepening of the intertidal circulation cell (feature 2), pushing freshwater discharge further offshore along with the lower interface and deep circulation cell (feature 3). The movement of the three flow paths during decreased freshwater flux is indicated with solid flow paths; dotted flow paths indicate movement of these features during increased freshwater flux. Both local and deep freshwater sources are shown. (B) Well map of the Cape Shores aquifer. Well annotation is given for sample nomenclature as well number and depth number (i.e., W1D1 means well 1, depth 1). Elevation is given as meters relative (rel.) to MSL.

In the intertidal zone, mixing of fresh and saline groundwater can lead to redox reactions responsible for Fe(II) oxidation and precipitation. This results in Fe minerals coating the sands of the beach aquifer (Charette and Sholkovitz 2002; Windom et al. 2006; Roy et al. 2010). Precipitation of solid Fe phases (e.g., $Fe^{III}OOH$) can significantly alter groundwater chemistry through adsorption and coprecipitation of groundwater-borne nutrients (e.g., phosphate) and toxins (e.g., arsenic) (Charette et al. 2005; Jung et al. 2009). This zone of reactive Fe minerals has been observed in several coastal aquifers, although its formation is not well understood. Suggested formation mechanisms include: mixing of anoxic Fe(II)-rich freshwater with oxygenated seawater (Charette et al. 2005; Windom et al. 2006), and changes in pH affecting the rate of Fe(II) oxidation at the fresh and saline mixing boundary (Spiteri et al. 2006). Determining the mechanism(s) is important for understanding the effect of groundwater mixing on the location and extent of the Fe-mineralized zone, especially as the residence times of immobilized solutes sequestered in this zone are dependent on its dynamics (Charette and Sholkovitz 2002; Charette and Sholkovitz 2006).

The cycling of dissolved and solid Fe(II) and Fe(III) species within the Fe-mineralized zone is likely the result of the interplay of geochemistry, hydrology, and microbial activity. Microorganisms are capable of coupling many redox reactions to energy production within the cell, catalyzing these processes at a faster rate than abiotic processes. Fe- and S-cycling microbial communities can affect, and potentially control, the formation and dissolution of Fe and S solid phases, including FeOOH, FeS, and FeS_2. Although the mixing of redox species should support diverse microbial communities within coastal aquifers, studies of microbial populations in this environment have thus far been limited to N-cycling microorganisms (Santoro et al. 2006; Santoro et al. 2008; Sáenz et al. 2012), as well as microorganisms transported through the aquifer (Boehm et al. 2004; Russell et al. 2012). Beyond these, we are unsure if and how microbial populations affect other solute loads carried by SGD. Do microorganisms drive Fe- and S-cycling in the intertidal mixing zone? If so, how do they interact with geochemical and hydrologic processes to influence Fe-mineralized zone formation and dissolution?

To answer these questions, we conducted an integrated microbial, geochemical, and hydrologic study at Cape Shores, Lewes, Delaware. We correlated microbial populations to geochemistry, identifying niches within the intertidal mixing zone where these microorganisms may affect the formation and dissolution of FeOOH and FeS minerals. By surveying microbial population identity, we show several distinct communities of Fe- and S-cycling microorganisms near the point of groundwater discharge. Integrating our microbial, geochemical, and hydrologic data, we discuss the processes by which Fe- and S-cycling microbial populations can affect the balance of dissolved and solid Fe and S species, leading to a dynamic Fe-mineralized zone.

Beach aquifer flow path dynamics at Cape Shores, Lewes, Delaware

This study took place in the intertidal mixing zone of the beach aquifer at Cape Shores, Lewes, Delaware (38˚47.13′N, 75˚6.27′W), a large, sandy spit located at the intersection between the Atlantic Ocean and the Delaware Bay. Previous studies have characterized the geochemistry (Ullman et al. 2003; Miller and Ullman 2004; Hays and Ullman 2007) and physical hydrology (Heiss et al. 2014; Heiss and Michael 2014). Groundwater flow in the beach aquifer is highly transient, responding to both inland and offshore dynamics. The salinity distribution in the beach aquifer responds most significantly to changes in the hydraulic gradient driving fresh groundwater flow, and also to changes in tidal amplitude

over spring-neap cycles and storm events (Heiss and Michael 2014). During periods of low hydraulic gradients (low freshwater flux), the intertidal circulation cell (Fig. 1A, feature 2) expands both horizontally and vertically, and then contracts during periods of high gradients and associated high freshwater flux. This motion results in corresponding shifts in both the zone of fresh discharge and the lower interface (Fig. 1A, features 1 and 3; Heiss and Michael 2014), with the lower interface moving landward during periods of high freshwater flux (Fig. 1A, dotted lines) and seaward during periods of low freshwater flux (Fig. 1A, solid lines). As hydraulic gradients shift on these monthly and seasonal freshwater flux cycles, solute composition and flux to particular locations change, potentially causing reactions with the immobile mineral coatings. Thus, changes in the mixing zone hydrology can have a large effect on the geochemistry of pore water and solid phases in the beach aquifer.

Methods

Dune well water table and hydraulic gradient

The water table elevation 23 m behind the dune (42 m from the beachface-mean sea level [MSL] intersection and landward of the extent of tidal inundation) was recorded at 15 min intervals for the five-month sampling period using a pressure sensor (Schlumberger Micro-Diver). Tide elevation was determined from the Lewes, Delaware tide gauge station one kilometer west of the pore water sampling transect. Hydraulic gradient was taken as the difference between the dune water table elevation and the tide elevation over the distance between the dune well and the MSL-beach intersection.

Pore water sampling

Pore water was sampled from the intertidal zone along a transect of eight long-term multilevel-sampling wells. The shore-perpendicular transect extended 37 m from the backshore to the first offshore sand bar and consisted of 33 ports that ranged in depth from 0.39 m to 3.6 m below the surface (Fig. 1B). Pore water sampling was performed monthly from June to October 2013 during monthly spring low tide. Previous research at this site has shown that the salinity distribution does not vary significantly over a semidiurnal tidal cycle (range of $\sim$ 1.4 m; Heiss and Michael 2014).

Sampling ports were attached to polyethylene tubing of 0.48 cm inner diameter. These were used to pump pore water from the subsurface using a peristaltic pump at a flow rate of 3.5–5.8 mL s^{-1}. For each well, sampling began at the deepest port and continued upward, finishing at the shallowest port. A volume of water at least three times the volume of the tube was pumped before the sample was collected to ensure that pore water measurements were representative of aquifer conditions.

Geochemical analysis

For all months but July, pore water was pumped directly into a 100 mL flow cell attached to a YSI Quatro containing probes to measure salinity, pH, oxidation-reduction potential, and temperature. These probes provided data to a YSI Professional Plus hand held meter to record measurements. The outflow of the flow cell was directed into another container where a SevenGo (Duo) OptiOx^{TM} dissolved oxygen probe was used to collect accurate oxygen readings (Mettler Toledo). In July, the pore water first flowed through an electrochemical cell to measure several redox species, including S species, Fe(II), Fe(III), Mn, O_2, and H_2O_2 (reactive oxygen species). The methods for instrument set up and use particular for this dataset have been described in detail by MacDonald et al. (2014).

Following the flow-through procedure, two sterile 50 mL centrifuge tubes were filled with pore water, taking care to prevent oxidation, and then analyzed for Fe(II), total Fe, and H_2S using a Hach DR 2000 spectrophotometer. H_2S was measured using the Hach methylene blue assay. In July and August, unfiltered total Fe was measured using the Hach FerroVer assay (1,10 phenanthroline method). In July, Fe(II) was measured after 0.22 μm filtration using the Hach Ferrous Iron Reagent (1,10 phenanthroline method). In August, Fe(II) was measured after 0.22 μm filtration by the ferrozine assay, modified with the addition of sample to 36 mmol L^{-1} sulfamic acid (Klueglein and Kappler 2013). We changed Fe(II) assay methods because processing of samples in the field took too long in July; therefore, in August, we preserved samples in sulfamic acid and performed the analyses in the laboratory. Comparison of total Fe and Fe(II) measurements indicated that the majority (74–98% average for each month) of the total Fe was Fe(II), with a matching distribution pattern. Samples for nitrate were taken in July, frozen, and later measured in triplicate through a flow through cell on a Submersible Ultraviolet Nitrate Analyzer (SUNA) V2 (Satlantic) after a deionized water and three-point 5 μM to 100 μM KNO_3 calibration. Nitrate measurements may be artificially higher from interference with dissolved organic matter. For all assays, the manufacturers' instructions were followed. Distributions of geochemical species were mapped onto the sampling transect and contoured using cubic interpolation in MATLAB.

Pore water microbial community sampling

Following geochemical sampling, one liter of pore water was pumped and sampled at a rate of 13.2 mL s^{-1}. This water was then filtered through 0.22 μm Sterivex filters to obtain concentrated samples for deoxyribonucleic acid (DNA) extraction (Millipore). Filters were loaded until pore water would no longer pass through, suggesting that organisms smaller than 0.22 μm would still be captured by this technique (although their relative abundance may be partially skewed). In June, filtering was conducted on the beach directly following the sampling of each port. In all other months, sterile, one liter containers were filled with pore water and stored on ice until field sampling was complete.

Samples were filtered on the same day at the lab. After filtering, all Sterivex filters were transported on dry ice and then stored at −80°C until DNA extraction.

DNA extraction

To determine microbial community composition through DNA sequencing, genomic DNA was extracted from Sterivex filters using a PowerSoil DNA Isolation kit (MoBio) following the manufacturer's instructions, except that gDNA was eluted into 10 mmol L^{-1} Tris at pH 8. Genomic DNA concentration and purity were measured using a Nanodrop ND-1000 before being stored at −20°C. All samples were extracted and frozen until the entire set was prepared for sequencing.

454 pyrosequencing

Quantification of bacterial relative abundance was accomplished through tagged pyrosequencing of the V1–V3 region of the small subunit (SSU) ribosomal ribonucleic acid (rRNA) gene. Extracted genomic DNA was sent for a single run of pyrosequencing at the Research and Testing Laboratory (Lubbock, TX, U.S.A.), with a second run of four samples to compare relative abundance across technical replicates, following their standardized protocol. In short, barcoded (eight base pairs) amplicons were constructed, pooled, purified, size selected, and sequenced on a Roche 454 FLX system with Titanium chemistry. Raw reads were denoised by the Research and Testing Laboratory pipeline.

Pyrosequencing data analysis

All data were analyzed utilizing the Quantitative Insights into Microbial Ecology (QIIME) pipeline (Caporaso et al. 2010). Multiplexed libraries were assigned reads based on barcode with quality filtering such that only those sequences between 200 and 700 base pairs, mean quality score above 30, minimum six ambiguous bases, maximum six homopolymer run, and 0 primer mismatches were allowed. Of a total of 446,180 sequences, 72,970 were discarded with this filter (16.4%).

Operational taxonomic units (OTUs), a functional classification for microbial "species," were chosen by a 97% identity cutoff using uclust, with reverse strand match. A total of 22,177 OTUs were called, and a representative set with one sequence from each OTU was chosen for downstream analysis from each cluster or OTU seed. This sequence subset was then classified into taxonomic groups using the SILVA next-generation sequencing (SILVAngs) pipeline (Quast et al. 2013). The OTU sequence subset was then aligned with the Python Nearest Alignment Space Termination (PyNAST) tool and chimeric sequences were identified with ChimeraSlayer (1036 total). Summary tables were then calculated removing these chimeric sequences, leaving 81.4% of the starting sequences after quality filtering. For the pore water samples, after quality filtering the total sequences per sample ranged from 1104 to 9519 sequences (avg. 3815 sequences). The total number of OTUs per sample ranged from 225 to 2089 OTUs (avg. 778 OTUs). Comparison of Zetaproteobacteria relative abundance determined from separate quantitative polymerase chain reaction (Q-PCR) analysis (method from Fleming et al. 2013) to the results from pyrosequencing analysis found a strong correlation ($R^2 = 0.91$) at a near 1 : 1 ratio (slope = 1.08), indicating good agreement in microbial relative abundance between methods. The four technical replicates from the second pyrosequencing run were also in good agreement with the main pyrosequencing run.

Microbial community diversity

We used the QIIME pipeline to calculate beta diversity metrics. Beta diversity was used to calculate a weighted unifrac distance metric to perform unweighted pair group method with arithmetic mean (UPGMA)-based cluster analysis of microbial communities based on phylogenetic distance of all quality-filtered sequences. The metabolic diversity of Fe- and S-cycling microbes was determined by mapping the top 1% of all taxa to representatives with known metabolic function. This was done only at the genera level using primary literature, so that we could identify microbes for discussion. Metabolic assignments had no impact on biological groupings determined by unifrac analysis.

Statistical analyses

Microbial community structure was further examined using nonmetric multidimensional scaling (NMDS), a nonparametric (i.e., based on rank order) ordination technique that is not dependent on or adversely affected by nonnormality or related data structure issues. Bray–Curtis percent dissimilarity values (normalized) were used as the data distance input matrix. NMDS analyses were conducted using the MDS procedure in SAS/STAT® Software (version 9.3; SAS Institute). Community structure was explored at the class taxonomic level using relative abundances, filtering out microbes of extreme low relative abundance (< 0.5%). Including these "rare" taxa occurrences can bias NMDS analyses by emphasizing within-site uniqueness at the expense of between-site similarities. The appropriateness of a NMDS result, or the degree to which a given solution is representative of the original input data matrix, was assessed using the stress or badness-of-fit statistic (on a scale of 0 to 1, with 0 indicating perfect ordering between input data and a NMDS solution).

The variability in the data explained by an NMDS dimension was assessed using an R^2 value from a regression of the individual dimension scores vs. the original data matrix distance values. Spearman rank correlation was used to assess which specific geochemistry data were related to a particular NMDS output. Significant correlations ($\alpha = 0.11$ for chemistry; $\alpha = 0.05$ for taxa relative abundance) between NMDS dimension scores and geochemistry or taxa relative abundance values offer evidence of driving factors behind bacterial community structure in this study.

Sample groupings suggested by the unifrac analyses and supported by the NMDS results were statistically

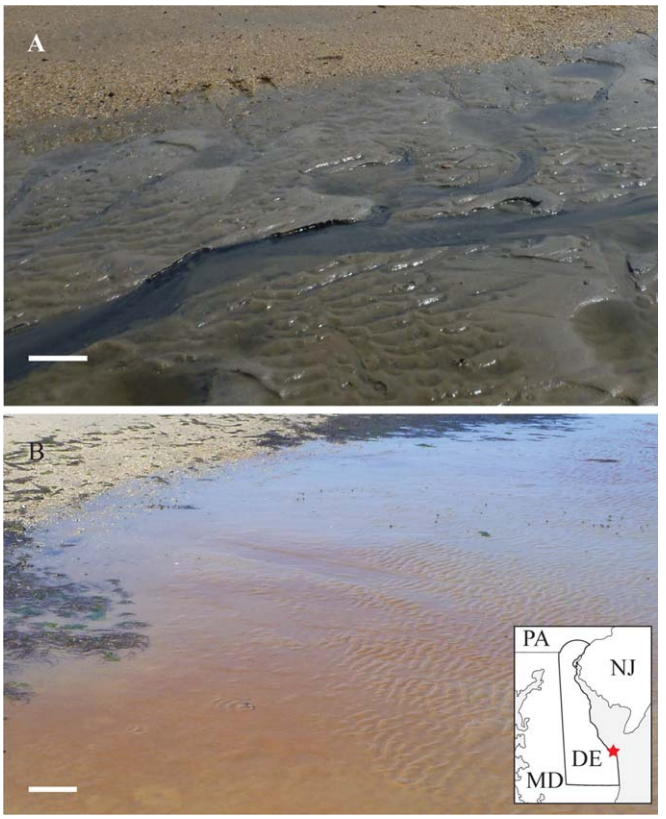

Fig. 2. Fe and S solid phases were visible at the point of discharge at low tide (between wells 6 and 7), showing variable mineralogy as (A) FeS in July and (B) FeOOH in August. Inset shows location of sampling at the state level. Scale bars = 10 cm.

corroborated via Multiple-Response Permutation Procedures (MRPP; PC-ORD™, version 6.0, MjM Software Design) at a significance level of $\alpha = 0.05$. The same data distance matrix input was used for NMDS and MRPP analyses, using rank-transformed, Bray–Curtis percent dissimilarity values. The MRPP test statistic (A) provides an indication of within-group homogeneity. A maximum value of 1 implies all items within a group are identical. Conversely, $A = 0$ indicates group heterogeneity expected by chance; values < 0 imply less agreement within groups than expected by chance.

Nucleotide submission

Raw sequence data was submitted to the sequence read archive (SRA) at the National Center for Biotechnology Information (NCBI), with all appropriate metadata under project accession SRP042362.

Results

At the Cape Shores field site, an extensive Fe-mineralized zone is inferred from the distribution of pore water geochemistry. Observed monthly (i.e., every other spring tide), the geochemistry responded to a dynamic hydrologic environment, ultimately affecting microbial populations, and having a visible effect on the mineral coatings on sands at the point of discharge (Fig. 2A, FeS; Fig. 2B, FeOOH). Due to the more thorough characterization of geochemistry in July, including electrochemical measurements, we will focus our results and discussion around this month. Following this, we will discuss differences observed between July (high freshwater flux) and August (low freshwater flux). The dynamic nature of the intertidal mixing zone is evident in the changes in hydrology, geochemistry, and microbiology between these two months.

Beach groundwater dynamics

Pore water salinity measurements confirmed the presence of the intertidal circulation cell found in previous studies (Fig. 3B; Heiss and Michael 2014). Variability in the horizontal and vertical extent of the intertidal circulation cell and

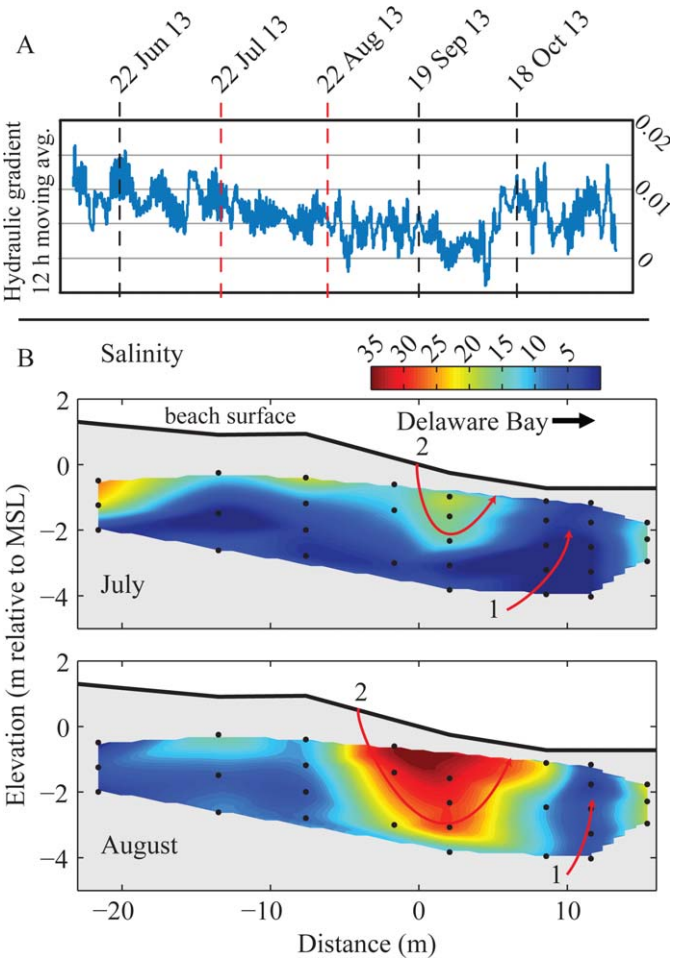

Fig. 3. (A) Hydraulic gradient for sampling period, showing the general trend of decreasing freshwater supplied to the intertidal mixing zone over the summer months. A hydraulic gradient > 0 means groundwater flux is toward the bay. Dashed lines show sampling dates, with July and August (discussed in text) in red. (B) Salinity color maps from July and August. Variations in the depth and extent of the intertidal circulation cell (arrow 2) respond to changes in freshwater flux and affect the location of the freshwater discharge flow path (arrow 1).

the width of the fresh discharge zone led to changes in the location and extent of mixing between fresh and saline groundwater. These differences were likely driven by variations in the terrestrial hydraulic gradient (Fig. 3A). The dune water table was highest and freshwater gradient strongest during the July sampling. The greater flow of fresh groundwater through the system during this time period reduced seawater infiltration and resulted in a smaller circulation cell and lower salinity (Fig. 3B). In August, the dune water table and thus freshwater flow were lower. This allowed infiltrating seawater to penetrate deeper into the aquifer. The high salinity beneath the backshore at −22 m may be explained by occasional saltwater overtopping into a low lying area in the backshore. The shifting salinities between July and August highlight the dynamic nature of the groundwater flow and salinity in the beach aquifer.

Mixing zone geochemistry

The observation of key redox species (e.g., O_2, Fe(II), Fe(III), H_2S, and NO_3^-) and master control variables (e.g., pH, temperature, and salinity) allows us to determine the redox zonation of the intertidal mixing zone. This helps us to predict favorable geochemical reactions and infer the location and extent of the Fe-mineralized zone. Geochemical zonation is also necessary to understand the activity of microbial communities.

To visualize this redox zonation, geochemical and physical parameters were mapped for July (Fig. 4) and August (Fig. 5). By overlaying these data (Fig. 6), we can highlight geochemical reactions along freshwater and saline flowpaths. Oxygen is brought into the aquifer from surface ocean water infiltration, and is highest at the shallowest depths, although still only at 31% oxygen saturation (78 μmol L^{-1}; Fig. 4A). In the freshwater region (salinity < 5), oxygen is still present

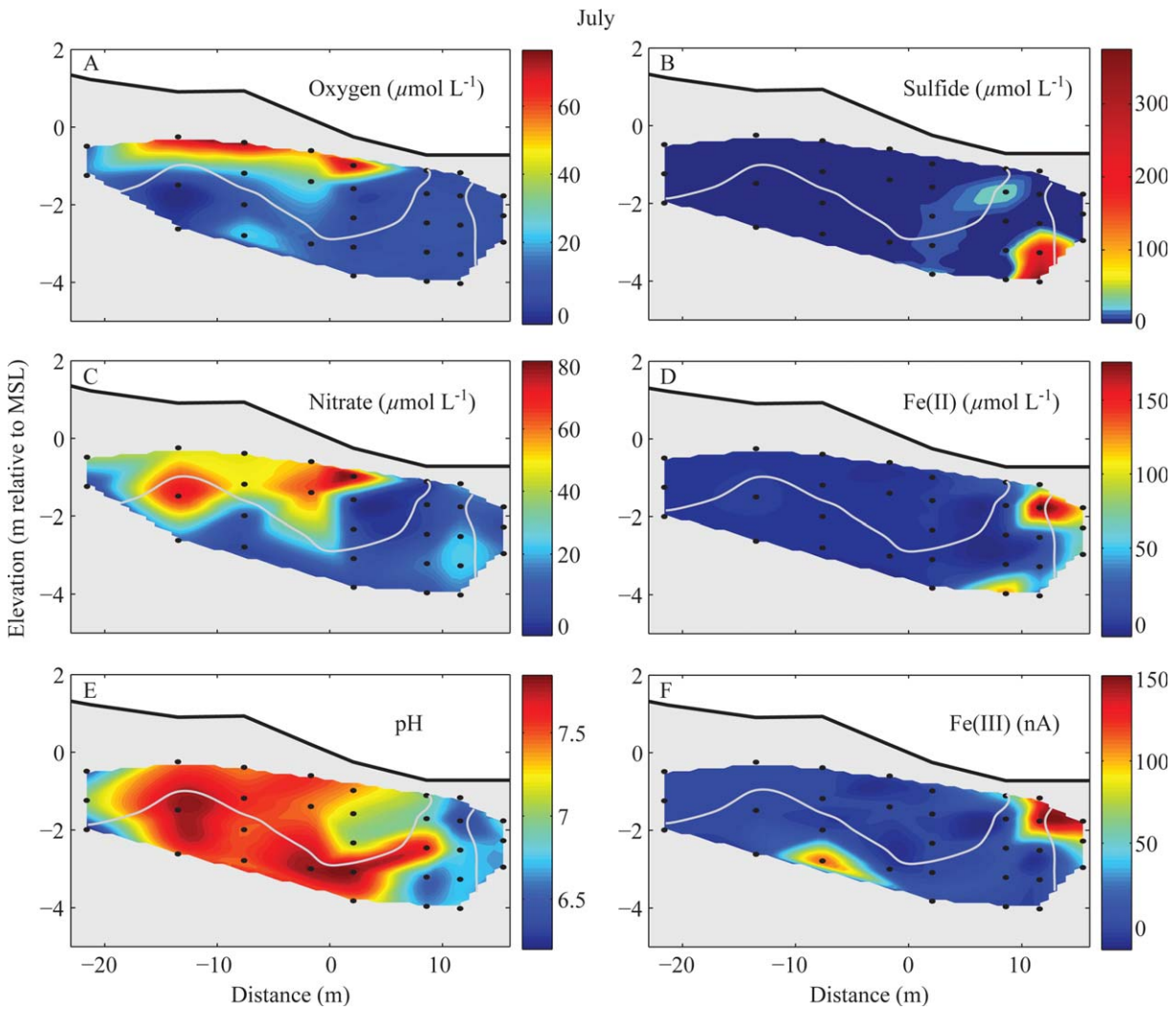

Fig. 4. July pore water chemistry parameters color maps. (A) O_2, (B) sulfide, (C) nitrate, (D) Fe(II), (E) pH, and (F) Fe(III), are shown. Units for Fe(III) are given as current (nanoamps; nA) as a calibration standard cannot be made. A contour at salinity of 5 is shown in gray to highlight the location of the freshwater discharge flow path.

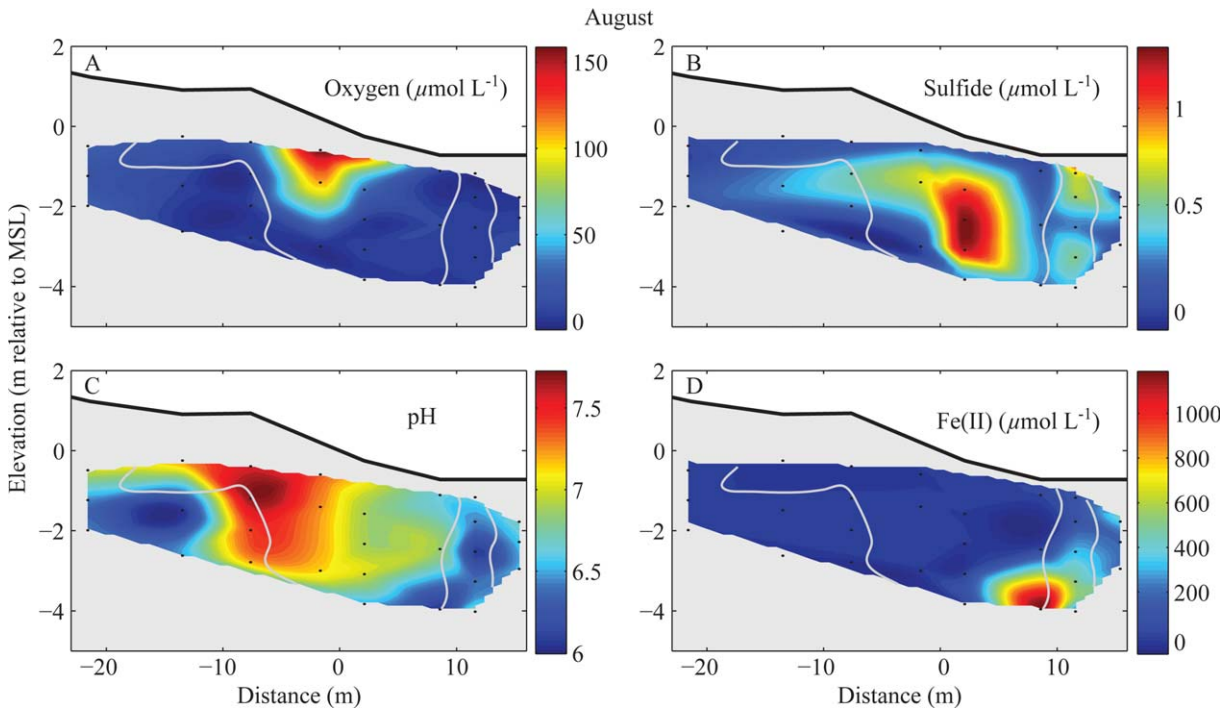

Fig. 5. August pore water chemistry parameters color maps. (A) O_2, (B) sulfide, (C) pH, and (D) Fe(II) are shown. A contour at salinity of 10 is shown in gray to highlight the location of the freshwater discharge flow path.

at low concentrations, averaging 6.4 μmol L^{-1}. The distribution shows that oxygen is consumed with depth across flow paths starting in near-surface pore waters, and is still available as an electron acceptor within the Fe-mineralized zone. Nitrate concentrations increased with depth until 2.4 m, after which it was depleted to below detection (<2 μmol L^{-1}). The source of the nitrate is likely from organic matter degradation. In August, the distribution of oxygen in the surface aquifer and low oxygen concentrations within the freshwater flow path (averaging 6.0 μmol L^{-1}) are similar to the July data (Fig. 6).

Hotspots of Fe and S cycling were found toward the offshore end of the beach along the lower interface and within the discharging zone of fresh groundwater (Figs. 4–6). The sulfide maximum in S-rich region B interrupted the upper and lower Fe maxima (Fe-rich regions A and C), although 12 μmol L^{-1} to 23 μmol L^{-1} Fe(II) was still detected in this region (Fig. 6A). Another sulfide maximum was measured downgradient of the bottom of the intertidal circulation cell (Fig. 4B), likely derived from a different source than in S-rich region B. The sulfide maxima were located in similar regions in August, although concentrations were much lower than in July (1.3 μmol L^{-1} compared to 466 μmol L^{-1}). We infer that the enriched sulfide concentrations in July are real, particularly considering FeS dominated the mineral-coated sands at the point of discharge in July (Fig. 2A) as opposed to FeOOH coated sands in the other months (Fig. 2B). However, the difference may be exaggerated since cyclic voltammetry data (July) is collected in line, preventing sulfide oxidation while spectrophotometry (August) is performed on water samples exposed to air before processing, although care was taken to minimize this effect. FeS nanoparticles were qualitatively detected between regions A and B through cyclic voltammetry (Fig. 6A). The distribution of dissolved Fe(II), Fe(III), H_2S, and FeS within pore water along the lower saline interface (between the most seaward wells, 7 and 8) can be used to infer the location of the Fe-mineralized zone.

Microbial community identity and function

To assay microbial relative abundance and connect their identity to metabolic function, we sequenced a region of the conserved SSU rRNA gene and used metabolic information from known isolates to predict function. While inactive microorganisms may be detected, groundwater flow would remove dead microbes from a porewater niche (*see* descriptions below) within a week (1.6 m d^{-1} flow rate). Detailed sequence classifications are available for viewing in an interactive hierarchical data browser (Fig. A1; *see* the supplemental materials). For all samples, Proteobacteria was the dominant phylum and constituted 37% of all sampled microbial communities, followed by Bacteroidetes (14%) and Chloroflexi (9%). The top four taxa reported from each pore water group were dominated by: (1) members of the Delta- and Gammaproteobacteria, (2) uncharacterized candidate division OP3, and

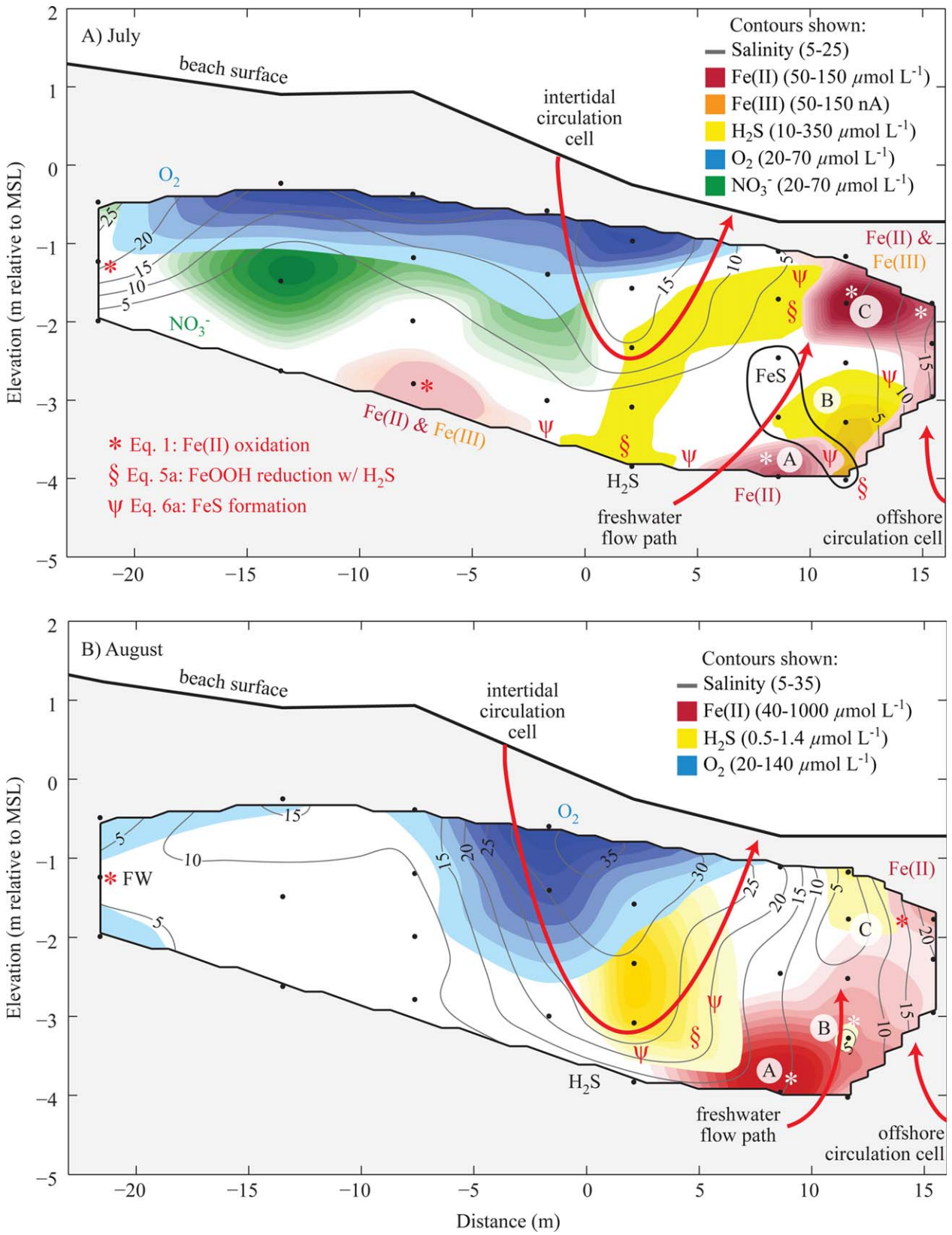

Fig. 6. Contour plots from (A) July and (B) August pore water sampling showing the distribution of O_2, sulfide, nitrate, Fe(II), and Fe(III). Low and high contoured values are given for each parameter. Concentrations outside the contoured area are below the minimum contour value, and are not necessarily zero (e.g., O_2 is not zero below the 20 μmol L^{-1} contour). Salinity contours are overlaid in gray. The three primary flow path features are identified by red arrows. The lower saline interface can be seen between wells 7 and 8. Circled letters indicate regions of interest that are referred to in text. Suggested locations for key chemical reactions are indicated with symbols.

(3) two orders of the Chloroflexi (Anaerolineae and Caldilineae; Fig. 7). As one of the most thoroughly characterized phyla, classifications within the Proteobacteria provide the most information for predicting metabolic function.

Fe- and S-cycling microbes were identified based on the metabolic characteristics of closely-related isolates. Sulfate reducers were dominated by members of the Deltaproteobacteria order Desulfobacterales (Kuever et al. 2005). In particular, *Desulfovibrio, Desulfopila*, and *Desulfurispora* were the most commonly represented genera, up to 29% in communities supported by the influx of sulfate from the saline intertidal and deep circulation cells. In the shallow aquifer, S-oxidizers in the Alphaproteobacteria and Epsilonproteobacteria were enriched to 14%, most notably the *Thioclava* and *Sulfurimonas* genera, respectively (Inagaki et al. 2003; Sorokin et al. 2005).

Fe(III)-reducers were found at a maximum relative abundance of 2.5% in pore waters both toward the surface and at depth. These included the genera *Geopsychrobacter* and *Geobacter* from the Deltaproteobacteria (Lovley et al. 1993; Holmes et al. 2004). In pore waters, known Fe(II)-oxidizers *Mariprofundus* (Zetaproteobacteria) and *Ferritrophicum* (Betaproteobacteria) were common only up to 3–8% relative abundance (Weiss et al. 2007). Within surface sediments at the point of SGD, however, Fe(II) oxidation was identified in highest relative abundance (up to 14% of the total community) within the linings of worm burrows, where the Fe(II)-oxidizing *Mariprofundus* genus (Zetaproteobacteria) were dominant with the majority of detected OTUs novel from those previously reported (Emerson et al. 2007; McAllister et al. 2011).

Microbial community clustering and niche determination

Clustering of pore water samples by microbial community similarity allows us to determine how microbial communities are associated with Fe, and what conditions affect community composition. Unifrac cluster analysis based on phylogenetic distance and OTU (equivalent to uncultured microbial species) relative abundance of all quality-filtered sequences grouped the microbial communities of the intertidal mixing zone into several pore water groups. Here, we focus on the five major groups found within the Fe-mineralized zone plus one group representing the upgradient freshwater environment (Fig. 7). These phylogeny-based sample groupings are supported by the NMDS analysis (Fig. 8), and are statistically distinct groupings based on the MRPP analysis ($A = 0.59$; p-value < 0.00001).

Fe(II), total Fe, salinity, and oxygen concentrations were significantly correlated ($\alpha = 0.11$) with microbial community structure in the intertidal mixing zone based on the NMDS analysis (Fig. 8). Each pore water group is associated with a niche, differentiated by Fe or S concentrations and salinity (Figs. 6–8). Salinity consistently separates pore water groups 3 and 4 (high salinity) from pore water groups 1, 2, and 5 (low salinity; Fig. 8). Further, pore water groups 2 and 3, and some of the samples from group 1, were associated with high Fe concentrations while pore water groups 4 and 5 were found primarily in shallow pore water samples near the point of discharge in a high sulfide environment. Pore water groups 1, 2, and 3 were enriched in division OP3, with pore water group 2 showing a bloom in OP3 relative abundance in August (Fig. 7C), corresponding to an increase in Fe concentrations in well 7 from July to August (Fig. 6). Finally, we found a distinct community enriched in Fe(II)-oxidizing Betaproteobacteria in the upgradient freshwater environment of well 1, of which a single sample (labeled FW) is represented in Fig. 7A. This is the only location in the aquifer where we found a substantial concentration of known Fe(II)-oxidizers, although low levels of marine Fe(II)-oxidizers were found in the Fe-mineralized zone (Fig. 7B,C).

Many of the pore water microbial groups were dominated by members of unknown metabolic capability, most notably candidate division OP3. Communities within Fe-rich regions in both freshwater and saline conditions were dominated by this uncharacterized phylum. Its enrichment in these environments suggests that it plays a role in Fe-cycling. Also of note is that every pore water sample had a significant portion of the microbial community corresponding to sulfate-reduction, making this the predominant recognized metabolism within the intertidal mixing zone.

Discussion

Within the Cape Shores beach aquifer, a zone enriched in dissolved Fe and sulfide forms just below the point of groundwater discharge. This is consistent with previous observations of dissolved and solid Fe phases in intertidal zones of beach aquifers (Charette and Sholkovitz 2002; Beck et al. 2010; Roy et al. 2010). The accumulation of Fe(II) in the pore water implies both a source of Fe(II) to this zone of the aquifer and a localized Fe(II) source, which must be Fe(III)-coated sands. The location near the discharge zone suggests that Fe mineral-controlled chemical sequestration and release (e.g., adsorption, coprecipitation, dissolution) represent significant mechanisms for altering the groundwater chemical load just prior to discharge. Thus, to understand controls on SGD chemistry, we now assess how these Fe(II) and Fe(III) minerals form, and what factors regulate their formation.

This Fe-mineralized zone is located at the convergence of the intertidal circulation cell, deep circulation cell, and freshwater flow path (Fig. 6), which introduce different sources of organic C, sulfate, Fe(II), and Fe(III) into the beach aquifer. Here, we examine how the interplay of hydrology, geochemistry, and microbiology affects these inputs and subsequent reactions that ultimately affect the Fe-mineralized zone composition and extent. We infer specific abiotic reactions, and integrate microbial community results with kinetics calculations to demonstrate how microbial activity

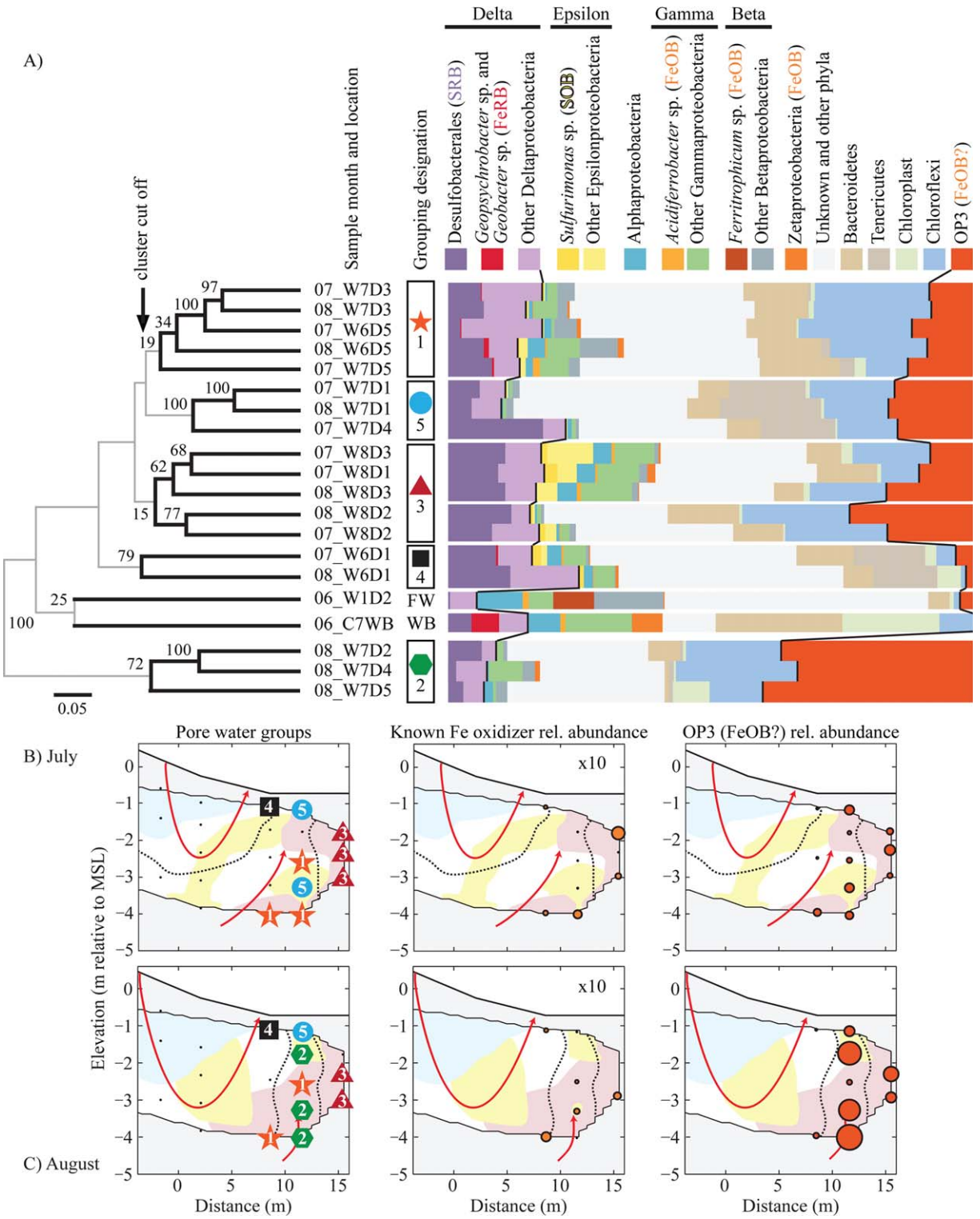

Fig. 7. (A) Cluster analysis of pore water samples based on microbial community phylogeny shows that communities sampled from niches with similar geochemistry harbor similar microorganisms. Numbers at nodes of the dendrogram are jackknife values indicating the confidence in the indicated node. Shown in part A are the distributions of the six Proteobacterial classes, taxa with known metabolisms, and other relevant phyla for each designated pore water group as well as the worm burrow and upgradient freshwater samples. Highlighted microbial taxa include the Deltaproteobacteria, dominated by sulfate-reducing bacteria, and candidate division OP3, a potential Fe(II)-oxidizer. The spatial organization of microbial pore water groups and these highlighted taxa are shown for (B) July and (C) August. FeOB = Fe(II)-oxidizing bacteria; FeRB = Fe(III)-reducing bacteria; SOB = sulfur-oxidizing bacteria; SRB = sulfate-reducing bacteria; FW = upgradient freshwater environment; WB = worm burrow from surface sediment.

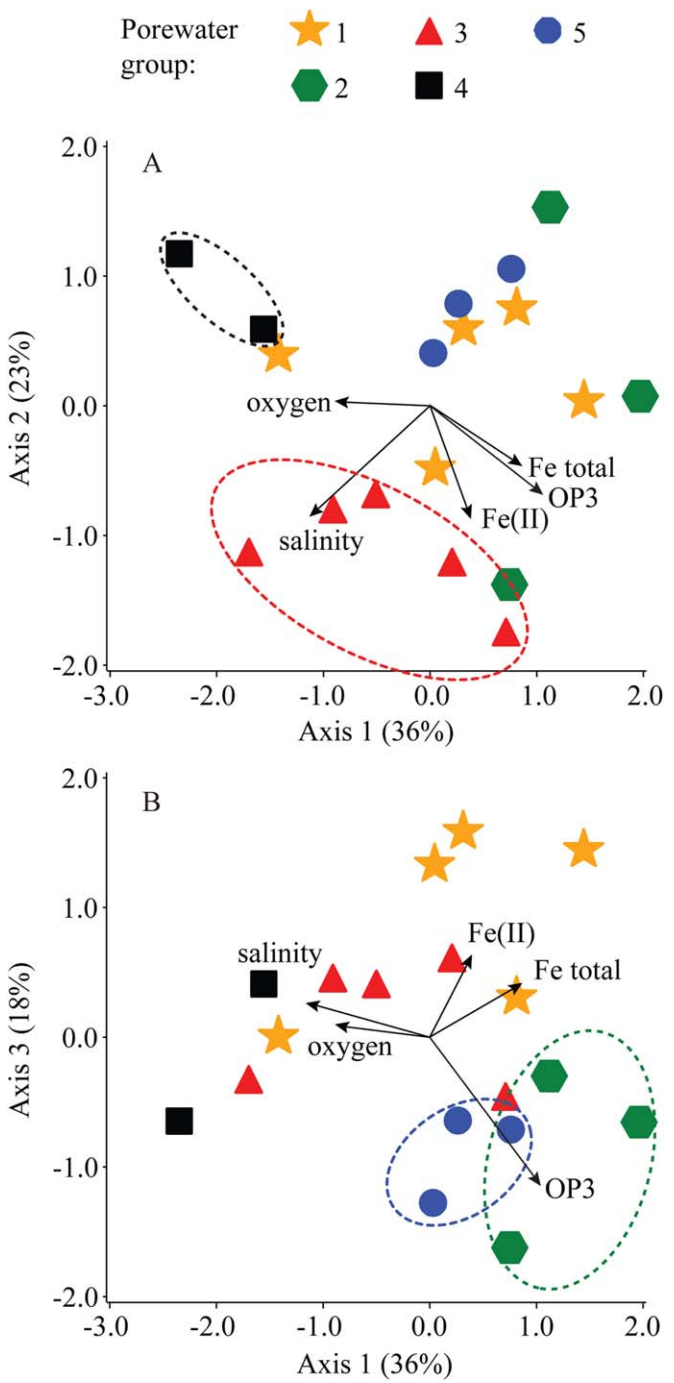

Fig. 8. NMDS plot showing microbial community structure. Pore water groups were determined by the unifrac phylogenetic comparison in Fig. 7. The three-dimensional solution (stress = 0.12) based on taxa relative abundance is shown in two separate scatterplots, with pore water groups circled in the plot that best shows sample grouping. Only statistically significant chemical correlations are shown. OP3 also significantly correlates with the community structure; other taxa were also statistically significant, but are not shown for clarity.

plays significant roles in Fe(III) oxyhydroxide (FeOOH) formation and transformation to FeS. We then show how the biogeochemistry reacts to changes in physical hydrology, which ultimately affects the location and extent of the Fe-mineralized zone.

Sources and reactions that provide sulfide and Fe(II) to the Fe-mineralized zone

Fe mineral composition and spatial distribution depends on the sources and relative fluxes of O_2, Fe(II), Fe(III), and sulfide, so we need to know how these chemical species are supplied to the Fe-mineralized zone. Seawater supplies S in the form of sulfate, along with oxygen and organics from primary producers. Surface sediment sequence analysis (Fig. A1; *see* the Web Appendix) showed that one source of organic carbon to the intertidal mixing zone was decomposed diatoms, detected through chloroplast sequences (Fig. 7A). In the intertidal circulation cell, this organic carbon is oxidized, coupled to the reduction of oxygen, then nitrate, and finally sulfate, producing sulfide. We infer a similar series of redox reactions ending with sulfate reduction in the deep circulation cell, although this cell occurs primarily outside of our sampling area.

Most of the Fe must come from fresh groundwater, yet we did not detect dissolved Fe(II) upgradient from the mineralized zone. Low Fe(II) concentrations could supply adequate Fe to the Fe-mineralized zone, if there is sufficient flux. A low Fe(II) flux is suggested by the presence of a significant Fe(II)-oxidizing community near the most landward well in June (up to 7.7% *Ferritrophicum* sp.) despite the apparent lack of Fe(II). Although it seems that Fe(II)-oxidizers would need more Fe(II), concentrations less than 3 μmol L^{-1} have been shown to support Fe(II)-oxidizing microbial communities (MacDonald et al. 2014). A more significant Fe(II) source could be deep anoxic freshwater, as suggested by previous research (Charette et al. 2005). Our sampling ports did not extend into an anoxic zone, but it is certainly plausible that Fe(II)-rich anoxic water lies beneath our sampling area. We thus infer that Fe(II) is sourced from deep freshwater, with some contribution from shallow groundwater.

Formation of the FeOOH component of the Fe-mineralized zone

Fe mineral coatings in an intertidal aquifer have previously been identified as the Fe(III) oxyhydroxides ferrihydrite, goethite, and lepidocrocite (Charette et al. 2005). FeOOH formation by aerobic Fe(II) oxidation follows the reaction:

$$Fe^{2+} + O_2 + 2H_2O \rightarrow FeOOH + O_2^- + 3H^+ \quad (1)$$

While we cannot detect FeOOH by sampling pore water, we can measure the acidification and reactive oxygen species

formation. Indeed, pH is an order of magnitude lower where we find dissolved Fe(II) and Fe(III) along the lower interface (Fig. 4E). In addition, we also measured H_2O_2 (43 μmol L^{-1}), which can form as the superoxide (O_2^-) product from Eq. 1 quickly reacts with Fe(II) or Mn(II) (Luther 2010; Hansard et al. 2011; Murphy et al. 2014). These findings are consistent with FeOOH formation along the lower saline interface. The lower pH within the fresh discharge zone and lower interface is inconsistent with the mechanism proposed by Spiteri et al. (2006), where higher pH from mixing with seawater was suggested to lead to a higher rate of abiotic Fe(II) oxidation, leading to the formation of the Fe-mineralized zone.

FeOOH formation by Fe(II) oxidation occurs via either abiotic or microbially mediated reactions. The mechanism that dominates depends on the relative rates of abiotic vs. biotic reactions. Here, we show that abiotic oxidation rates are relatively low under the measured aquifer conditions, compared to the range of microbial Fe(II) oxidation rates documented in the literature.

We can calculate the rate of chemical abiotic Fe(II) oxidation as:

$$-\mathrm{d}[Fe^{2+}]/\mathrm{dt} = k[Fe^{2+}][O_2][OH^-]^2 \quad (2)$$

where k, the overall reaction rate constant was calculated to range from 4×10^{14} mol^{-3} kg^3 min^{-1} at 27.0 salinity to 1×10^{16} mol^{-3} kg^3 min^{-1} at 0.09 salinity using equations from Millero et al. (1987). Using these calculated rate constants, we found that the abiotic Fe(II) oxidation rate was very slow, ranging from 2×10^{-4} μmol L^{-1} min^{-1} to 2×10^{-2} μmol L^{-1} min^{-1} for July (5×10^{-3} μmol L^{-1} min^{-1} average). This slow rate is primarily due to the low oxygen concentrations (average 6 μmol L^{-1}) found within the Fe-mineralized zone.

To compare the abiotic Fe(II) oxidation rates to previously measured microbial oxidation rates, we need to convert the overall reaction rate constant (k) to the pseudo-first-order rate constant (k_1):

$$k_1 = k[OH^-]^2[O_2] \quad (3)$$

For a particular pH and oxygen concentration, the Fe(II) oxidation rate is

$$-\mathrm{d}[Fe^{2+}]/\mathrm{dt} = k_1[Fe^{2+}] \quad (4)$$

Values of k_1, and correspondingly, abiotic Fe(II) oxidation rates, are lower at low O_2 concentrations and pH. We calculated abiotic k_1 values from 1×10^{-6} min^{-1} to 4×10^{-2} min^{-1} (5×10^{-3} min^{-1} average). To compete with abiotic Fe(II) oxidation, neutrophilic aerobic Fe(II)-oxidizing microbes have adapted to live in low oxygen environments, where biotic Fe(II) oxidation can proceed faster than abiotic Fe(II) oxidation (Roden et al. 2004; Rentz et al. 2007; Druschel et al. 2008). Comparing our calculated abiotic k_1 values to reported biotic k_1 values, we find that biotic rates are higher, by up to five orders of magnitude (2×10^{-2} min^{-1} to 4×10^{-1} min^{-1}) considering natural (Rentz et al. 2007), microcosm (Emerson and Revsbech 1994; James and Ferris 2004), and engineered systems (Søggard et al. 2001; Neubauer et al. 2002). If microbes oxidize Fe(II) at similar rates in the intertidal Fe-mineralized zone, they are likely significant or principal contributors to FeOOH formation.

Microbial Fe(II) oxidation in the intertidal mixing zone: A potential role for OP3?

Known Fe(II)-oxidizing microbes were detected in Fe(II)-rich areas of the intertidal mixing zone at low relative abundance (Fig. 7B,C). The highest relative abundances of known Fe(II)-oxidizers in pore water occurred within the freshwater (FW) upgradient pore water representative (freshwater; *Ferritrophicum* sp.) and pore water group 3 (saline; Zetaproteobacteria). While pyrosequence relative abundance does not necessarily correspond to activity, Fe(II)-oxidizers are not nearly as abundant as sulfate-reducers, leading us to wonder if microbial Fe(II) oxidation is not as important as we hypothesized above. However, we are likely overlooking many Fe(II)-oxidizers because we do not recognize them in our pyrosequence library. There are relatively few identified neutrophilic Fe(II)-oxidizers; these mostly come from freshwater or offshore marine environments (Emerson et al. 2010; McBeth et al. 2013), not brackish or estuarine water, with one exception (McBeth et al. 2011, 2013). We do find known marine Fe(II)-oxidizing microbes within the intertidal mixing zone, although not in the subsurface pore waters. Worm burrow samples taken in the top meter of the aquifer had a much higher relative abundance (up to 14% of the total community) of known Fe(II)-oxidizers. This abundance might be expected, considering the similarity between the high salinity, O_2-enriched worm burrow habitat and the steep redox gradients of previously studied marine sites. The deeper pore water environments, however, differ significantly from previously studied Fe(II)-oxidizer habitats (e.g., in salinity, physical setting), and therefore, we could expect them to host novel, yet-to-be discovered Fe(II)-oxidizing microbes.

Fe(II)-oxidizers could belong to one or more of the many taxonomic groups that could not be assigned a metabolism; these unassigned groups represent the majority of the sequences. Although we cannot say for certain which represent Fe(II)-oxidizers, our cluster analyses show that certain taxa are associated with the Fe-mineralized zone. In particular, all of the pore water groups found at depth (1, 2, and 3) were dominated by Candidate Division OP3, suggesting a major role for this microbe in the development of the Fe-mineralized zone. The most striking pattern of this division was in pore water group 2, where OP3 comprised approximately a third of the bacterial community. OP3 increased significantly from July to August in all samples within the

Fe-mineralized zone (Fig. 7B,C), particularly in region B, where we see a shift from high S to high Fe concentrations from July to August. This suggests that OP3 was enriched during the restoration of the FeOOH component of the Fe-mineralized zone (*see* below for discussion of FeOOH and FeS transformations).

Indeed, the OP3 division is often found where Fe- and S-cycling are common, in both freshwater and marine environments (Glöckner et al. 2010). To understand the diversity of our 1375 OP3 OTUs (out of 19,213 total OTUs recovered from this environment), we compared our sequences to a previously published phylogenetic survey that divided OP3 into five sublineages (Glöckner et al. 2010). We found that sublineages II and III were the predominant representatives in this study at 53% and 31%, respectively. Sublineage II, the dominant lineage in our samples, includes clones from Fe(II)-rich systems, including an Fe(II)-oxidizing freshwater biofilm (e.g., Genbank accession No. EU937932), deep sea Fe- and S-cycling microbial mats (Omoregie et al. 2008), and deep sea sediments (Li and Wang 2013). At our study site, OP3-dominated pore water groups 1, 2, and 3 are situated in low-sulfide, high dissolved Fe(II) regions along the lower interface (Fig. 7B,C). Considering these observations, it is possible that OP3 sublineages II and III are involved in Fe-cycling.

Sulfate reducers produce sulfide, which reacts with FeOOH to form FeS

Sulfate-reduction is the most commonly detected microbial metabolism in all regions of this site, with the activity evident as dissolved sulfide. The spatial distribution of sulfide has limited overlap with Fe(II) and Fe(III) distribution because sulfide reacts with Fe, causing FeOOH dissolution, Fe(III) reduction, and FeS precipitation (Fig. 6). There are several regions where we see the interaction of Fe(II) and Fe(III) with sulfides. Here, we explain how these reactions help us to determine the composition and spatial extent of the Fe-mineralized zone. Like FeOOH, FeS minerals can sequester solutes (particularly metals), but differ from FeOOH in exactly which solutes and to what extent (Fan et al. 2013). Understanding the transformation of FeOOH to FeS, and therefore, being able to predict FeS distribution is key to understanding the chemistry of SGD.

H_2S supplied by sulfate reduction in the intertidal and deep circulation cells reduces FeOOH as follows:

$$\text{if } pH < pK_1 \quad 2FeOOH + H_2S \rightarrow 2Fe^{2+} + S^0 + 4OH^- \qquad (5a)$$

$$\text{if } pH > pK_1 \quad 2FeOOH + HS^- + H_2O \rightarrow 2Fe^{2+} + S^0 + 5OH^- \qquad (5b)$$

where the hydrogen sulfide acid dissociation constant pK_1 varies with salinity and temperature (Millero et al. 1988). pK_1 values ranged from 6.51 to 7.05, leading to different protonation states of sulfide in the freshwater discharge zone (H_2S) and the intertidal and deep circulation cells (HS^-). Regardless of sulfide speciation, as long as there is FeOOH, this process will continue to consume sulfide and produce dissolved Fe(II). Although Fe(II) could also be produced by Fe(III)-reducing microbes, we detected very low levels of Fe(III)-reducers; reductive FeOOH dissolution by sulfide is likely more significant here, especially given the extent of sulfate reducing bacteria in this system. Dissolved Fe(II) (e.g., regions A and C; Fig. 6) is thus a signature of FeOOH presence and reduction (Rouxel et al. 2008). Furthermore, sulfide should not accumulate in pore water until reactive FeOOH is depleted; thus H_2S-rich regions (e.g., S region B) likely lack reactive FeOOH.

The continued supply of H_2S can further react with FeOOH-derived Fe(II) (i.e., product of Eq. 5a,b) to form FeS:

$$\text{if } pH < pK_1 \quad Fe^{2+} + H_2S \rightarrow FeS + 2H^+ \qquad (6a)$$

$$\text{if } pH > pK_1 \quad Fe^{2+} + HS^- \rightarrow FeS + H^+ \qquad (6b)$$

The net reaction when Eqs. 5 and 6 are combined is:

$$\text{if } pH < pK_1 \quad 2FeOOH + 3H_2S \rightarrow 2FeS + S^0 + 4H_2O \qquad (7a)$$

$$\text{if } pH > pK_1 \quad 2FeOOH + 3HS^- \rightarrow 2FeS + S^0 + 3OH^- + H_2O \qquad (7b)$$

In this way, FeS replaces FeOOH as the mineral component of the Fe-mineralized zone. We can detect this transformation along the bottom of the intertidal circulation cell where sulfide is in the form HS^-, producing hydroxide and increasing pH (Eq. 7b; Fig. 4E). Although our methods are not sensitive to bulk solid FeS, we did verify FeS presence by electrochemical detection of nanoparticulate FeS at the lower saline interface (Fig. 6). Furthermore, we visually observed black FeS in sediment samples and in the July groundwater discharge (Fig. 2). (We recognize that pyrite (FeS_2) formation is also possible, but we have no pyrite data at present.) FeS should be generated at all boundaries of Fe(II)- and H_2S-rich pore waters. Given that these interfaces can be extensive (Fig. 6), FeS is likely more widespread than our limited observations. Thus, it could represent a significant component of the Fe-mineralized zone, in addition to FeOOH.

How the Fe-mineralized zone forms: a summary

Using the above principles, we can explain how the intertidal mixing zone hydrology, geochemistry, and microbiology work together to affect the shape and extent of the Fe-mineralized zone. Fe(II) oxidation begins as Fe(II)-rich deep anoxic freshwater is forced to mix with shallow, slightly oxic freshwater along the lower saline interface. At these low oxygen levels, Fe(II)-oxidizing microbes outcompete abiotic Fe(II) oxidation, forming the FeOOH of the Fe-mineralized zone. This is similar to a previously proposed oxidation mechanism for Fe-mineralized zone formation (Charette and Sholkovitz 2002; Charette et al. 2005; Charette and Sholkovitz 2006), except that we can now specify microbial involvement, and demonstrate that shallow fresh groundwater can also be a source of low levels of oxygen. Sulfate reduction occurs within

both the intertidal and deep circulation cells, making these flow paths sources of sulfide that transform FeOOH to FeS from both the landward and seaward directions (roughly, S region B and the bottom of the intertidal circulation cell). Thus, the Fe-mineralized zone is comprised of both Fe oxides and sulfides, with the distribution depending on the geometry of the intertidal circulation cell, which in turn depends on the relative fluxes of fresh and saline groundwater (*see* next section). The cycling of Fe oxides and Fe sulfides is dependent on the interplay of these chemical fluxes with active microbial communities, leading to a dynamic interaction of solid and dissolved phases. Roy et al. (2010, 2011, and 2013) also found FeOOH reduction and FeS precipitation in the Indian River Lagoon aquifer, although they focused on the organic carbon-driven mechanism of Fe(III) reduction. At Cape Shores, the near absence of known Fe(III)-reducers combined with the sulfide distribution suggests that sulfide-driven Fe(III)-reduction plays a more important role here. Some of the contrasts between our findings and the findings referenced above may be due to differences in stoichiometries of C : S : Fe : O_2 inputs, as well as differences in fresh and saline groundwater flux, related flow path geometries, and tidal and seasonal dynamics. However, the hydrologic and geochemical phenomena we observed are relatively common, so it is likely that microbially mediated sulfate reduction and Fe(II) oxidation also play significant roles in other intertidal aquifers.

Hydrologic fluctuations affect the location and composition of the Fe-mineralized zone and associated microbial communities

Because solute fluxes and groundwater mixing drive biogeochemical reactions, hydrologic forcing plays an important role in determining the extent and location of the Fe-mineralized zone. Variability in freshwater flux and sea level lead to fluctuations in the location of the freshwater flow path and the intertidal and deep circulation cells (Heiss and Michael 2014). Sulfide is produced by sulfate reduction in both saline circulation cells; therefore, the movement of these saline cells will affect the transport of sulfide to the Fe-mineralized zone. Decreased freshwater flux leads to the expansion of the intertidal circulation cell, bringing sulfate and organic carbon into areas previously saturated with fresh water. The increased reduction of FeOOH in the Fe-mineralized zone due to rising levels of H_2S (Eqs. 5a,b) would explain the increase in dissolved Fe(II) concentrations in the Fe-mineralized zone of the aquifer from July to August. In comparison, the high freshwater flux in July led to lower dissolved Fe(II) concentrations, likely due to the landward shift of the lower interface and greater sulfide input from the deep circulation cell into S region B (Fig. 6). Seasonal hydrologic fluctuations are larger than monthly changes: the lower interface shifts up to four meters landward in winter months relative to summer (Heiss and Michael 2014). Therefore, seasonal cycles should have a large effect on the Fe-mineralized zone, likely leading to the dissolution of the majority of the Fe-rich zone or causing the entire zone to move landward, or both. Combining our results with the previous site hydrologic characterization, we suggest that hydrology has a large effect on the supply of reductant to the Fe-mineralized zone.

The expansion and contraction of the intertidal circulation cell and the oscillation of the lower interface also significantly affect microbial populations in the Fe-mineralized zone, and therefore which organisms contribute to Fe-cycling. The main factors affecting microbial community composition are Fe, sulfide, O_2, and salinity, all of which are influenced by the relative flux of fresh and saline groundwater within the intertidal mixing zone. Thus, any oscillation in the freshwater and saline interfaces will alter the dominant microbial populations not only based on available Fe and S sources, but based on salinity as well. Therefore, understanding the dynamic hydrology of any intertidal mixing zone should allow us to predict the distribution of microbial communities that shape the Fe-mineralized zone.

Implications for solute discharge

The dynamics of the Fe-mineralized zone can have a significant effect on the chemical load delivered to coastal waters by SGD. FeOOH has a high affinity for both nutrients (e.g., phosphate) and toxins (e.g., As and Pb; Charette et al. 2005; Jung et al. 2009) while FeS sequesters toxins, such as As, Pb, Hg, Cd, U, and Tc (Jeong et al. 2010; Fan et al. 2013). Therefore, as FeOOH and FeS are formed or dissolved, certain chemicals will be sequestered while others are released. In this way, the dynamics of the Fe-mineralized zone affect the residence times and ultimately, the discharge of different chemicals. Here, we have developed a combined hydrologic, geochemical, and microbial understanding of Fe mineralization in the intertidal mixing zone, including specific geochemical reactions and microbial mechanisms. Knowledge of these complex interactions, which are likely occurring in coastal aquifers worldwide, is a critical step toward more quantitative prediction, as with reactive transport models, of how natural and anthropogenic forcing (e.g., sea level rise, groundwater extraction, and wastewater organic and nutrient inputs) will affect SGD composition and coastal ocean chemistry.

Web Appendix: Detailed sequence classifications.

References

Beck, A. J., J. K. Cochran, and S. A. Sañudo-Wilhelmy. 2010. The distribution and speciation of dissolved trace metals in a shallow subterranean estuary. Mar. Chem. **121**: 145–156. doi:10.1016/j.marchem.2010.04.003

Boehm, A. B., G. G. Shellenbarger, and A. Paytan. 2004. Groundwater discharge: Potential association with fecal indicator bacteria in the surf zone. Environ. Sci. Technol. **38**: 3558–3566. doi:10.1021/es035385a

Caporaso, J. G., J. Kuczynski, J. Stombaugh, K. Bittinger, F. D. Bushman, E. K. Costello, N. Fierer, A. G. Peña, et al. 2010. QIIME allows analysis of high-throughput community sequencing data. Nat. Methods **7**: 335–336. doi:10.1038/nmeth.f.303

Charette, M. A., and E. R. Sholkovitz. 2002. Oxidative precipitation of groundwater-derived ferrous iron in the subterranean estuary of a coastal bay. Geophys. Res. Lett. **29**: 1444. doi:10.1029/2001GL014512

Charette, M. A., E. R. Sholkovitz, and C. M. Hansel. 2005. Trace element cycling in a subterranean estuary: Part 1. Geochemistry of the permeable sediments. Geochim. Cosmochim. Acta **69**: 2095–2109. doi:10.1016/j.gca.2004.10.024

Charette, M. A., and E. R. Sholkovitz. 2006. Trace element cycling in a subterranean estuary: Part 2. Geochemistry of the pore water. Geochim. Cosmochim. Acta **70**: 811–826. doi:10.1016/j.gca.2005.10.019

Druschel, G. K., D. Emerson, R. Sutka, P. Suchecki, and G. W. Luther, III. 2008. Low-oxygen and chemical kinetic constraints on the geochemical niche of neutrophilic iron(II) oxidizing microorganisms. Geochim. Cosmochim. Acta **72**: 3358–3370. doi:10.1016/j.gca.2008.04.035

Emerson, D., and N. P. Revsbech. 1994. Investigation of an iron-oxidizing microbial mat community located near Aarhus, Denmark: Laboratory studies. Appl. Environ. Microbiol. **60**: 4032–4038.

Emerson, D., J. A. Rentz, T. G. Lilburn, R. E. Davis, H. Aldrich, C. Chan, and C. L. Moyer. 2007. A novel lineage of Proteobacteria involved in formation of marine Fe-oxidizing microbial mat communities. PLoS One **2**: e667. doi:10.1371/journal.pone.0000667

Emerson, D., E. J. Fleming, and J. M. McBeth. 2010. Iron-oxidizing bacteria: An environmental and genomic perspective. Annu. Rev. Microbiol. **64**: 561–583. doi:10.1146/annurev.micro.112408.134208

Fan, D., R. P. Anitori, B. M. Tebo, and P. G. Tratnyek. 2013. Reductive sequestration of pertechnetate ($^{99}TcO_4^-$) by nano zerovalent iron (nZVI) transformed by abiotic sulfide. Environ. Sci. Technol. **47**: 5302–5310. doi:10.1021/es304829z

Fleming, E. J., R. E. Davis, S. M. McAllister, C. S. Chan, C. L. Moyer, B. M. Tebo, and D. Emerson. 2013. Hidden in plain sight: Discovery of sheath-forming, iron-oxidizing Zetaproteobacteria at Loihi Seamount, Hawaii, USA. FEMS Microbiol. Ecol. **85**: 116–127. doi:10.1111/1574-6941.12104

Glöckner, J., M. Kube, P. M. Shrestha, M. Weber, F. O. Glöckner, R. Reinhardt, and W. Liesack. 2010. Phylogenetic diversity and metagenomics of candidate division OP3. Environ. Microbiol. **12**: 1218–1229. doi:10.1111/j.1462-2920.2010.02164.x

Hansard, S. P., H. D. Easter, and B. M. Voelker. 2011. Rapid reaction of nanomolar Mn(II) with superoxide radical (O_2^-) in seawater and simulated freshwater. Environ. Sci. Technol. **45**: 2811–2817. doi:10.1021/es104014s

Hays, R. L., and W. J. Ullman. 2007. Direct determination of total and fresh groundwater discharge and nutrient loads from a sandy beachface at low tide (Cape Henlopen, Delaware). Limnol. Oceanogr. **52**: 240–247. doi:10.4319/lo.2007.52.1.0240

Heiss, J. W., and H. A. Michael. 2014. Saltwater-freshwater mixing dynamics in a sandy beach aquifer over tidal, spring-neap, and seasonal cycles. Water Resour. Res. **50**: 6747–6766. doi:10.1002/2014WR015574

Heiss, J. W., W. J. Ullman, and H. A. Michael. 2014. Swash zone moisture dynamics and unsaturated infiltration in two sandy beach aquifers. Estuar. Coast. Shelf Sci. **143**: 20–31. doi:10.1016/j.ecss.2014.03.015

Holmes, D. E., J. S. Nicoll, D. R. Bond, and D. R. Lovley. 2004. Potential role of a novel psychrotolerant member of the family *Geobacteraceae, Geopsychrobacter electrodiphilus* gen. nov., sp. nov., in electricity production by a marine sediment fuel cell. Appl. Environ. Microbiol. **70**: 6023–6030. doi:10.1128/AEM.70.10.6023-6030.2004

Inagaki, F., K. Takai, H. Kobayashi, K. H. Nealson, and K. Horikoshi. 2003. *Sulfurimonas autotrophica* gen. nov., sp. nov., a novel sulfur-oxidizing ε-proteobacterium isolated from hydrothermal sediments in the Mid-Okinawa Trough. Int. J. Syst. Evol. Microbiol. **53**: 1801–1805. doi:10.1099/ijs.0.02682-0

James, R. E., and F. G. Ferris. 2004. Evidence for microbial-mediated iron oxidation at a neutrophilic groundwater spring. Chem. Geol. **212**: 301–311. doi:10.1016/j.chemgeo.2004.08.020

Jeong, H. Y., K. Sun, and K. F. Hayes. 2010. Microscopic and spectroscopic characterization of Hg(II) immobilization by mackinawite (FeS). Environ. Sci. Technol. **44**: 7476–7483. doi:10.1021/es100808y

Jung, H. B., M. A. Charette, and Y. Zheng. 2009. Field, laboratory, and modeling study of reactive transport of groundwater arsenic in a coastal aquifer. Environ. Sci. Technol. **43**: 5333–5338. doi:10.1021/es900080q

Klueglein, N., and A. Kappler. 2013. Abiotic oxidation of Fe(II) by reactive nitrogen species in cultures of the nitrate-reducing Fe(II) oxidizer *Acidovorax* sp. BoFeN1—questioning the existence of enzymatic Fe(II) oxidation. Geobiology **11**: 180–190. doi:10.1111/gbi.12019

Kuever, J., F. A. Rainey, and F. Widdel. 2005. Order III. Desulfobacterales ord. nov., p. 959. *In* G. M. Garrity, D. J. Brenner, N. R. Krieg and J. T. Staley [eds.], Bergey's manual of systematic bacteriology, 2nd ed. Springer.

Li, T., and P. Wang. 2013. Richness and diversity of bacteria in the Nansha carbonate platform (Core MD05-2896), South China Sea. World J. Microbiol. Biotechnol. **29**: 1895–1905. doi:10.1007/s11274-013-1354-9

Lovley, D. R., S. J. Giovannoni, D. C. White, J. E. Champine, E. J. P. Phillips, Y. A. Gorby, and S. Goodwin. 1993. *Geobacter metallireducens* gen. nov. sp. nov., a microorganism capable

of coupling the complete oxidation of organic compounds to the reduction of iron and other metals. Arch. Microbiol. **159**: 336–344. doi:10.1007/BF00290916

Luther, III, G. W. 2010. The role of one- and two-electron transfer reactions in forming thermodynamically unstable intermediates as barriers in multi-electron redox reactions. Aquat. Geochem. **16**: 395–420. doi:10.1007/s10498-009-9082-3

MacDonald, D. J., A. J. Findlay, S. M. McAllister, J. M. Barnett, P. Hredzak-Showalter, S. T. Krepski, S. G. Cone, J. Scott, et al. 2014. Using *in situ* voltammetry as a tool to identify and characterize habitats of iron-oxidizing bacteria: From fresh water wetlands to hydrothermal vent sites. Environ. Sci. Process. Impacts **16**: 2117–2126. doi:10.1039/C4EM00073K

Martin, W. R. 2009. Chemical processes in estuarine sediments., p. 3549–3560. *In* J. H. Steele, K. K. Turekian and S. A. Thorpe [eds.], Encyclopedia of Ocean Sciences. Academic Press.

McAllister, S. M., R. E. Davis, J. M. McBeth, B. M. Tebo, D. Emerson, and C. L. Moyer. 2011. Biodiversity and emerging biogeography of the neutrophilic iron-oxidizing Zetaproteobacteria. Appl. Environ. Microbiol. **77**: 5445–5457. doi:10.1128/AEM.00533-11

McBeth, J. M., B. J. Little, R. I. Ray, K. M. Farrar, and D. Emerson. 2011. Neutrophilic iron-oxidizing "Zetaproteobacteria" and mild steel corrosion in nearshore marine environments. Appl. Environ. Microbiol. **77**: 1405–1412. doi:10.1128/AEM.02095-10

McBeth, J. M., E. J. Fleming, and D. Emerson. 2013. The transition from freshwater to marine iron-oxidizing bacterial lineages along a salinity gradient on the Sheepscot River, Maine, USA. Environ. Microbiol. Rep. **5**: 453–463. doi:10.1111/1758-2229.12033

Michael, H. A., A. E. Mulligan, and C. F. Harvey. 2005. Seasonal oscillations in water exchange between aquifers and the coastal ocean. Nature **436**: 1145–1148. doi:10.1038/nature03935

Miller, D. C., and W. J. Ullman. 2004. Ecological consequences of ground water discharge to Delaware Bay, United States. Ground Water **42**: 959–970. doi:10.1111/j.1745-6584.2004.tb02635.x

Millero, F. J., S. Sotolongo, and M. Izaguirre. 1987. The oxidation kinetics of Fe(II) in seawater. Geochim. Cosmochim. Acta **51**: 793–801. doi:10.1016/0016-7037(87)90093-7

Millero, F. J., T. Plese, and M. Fernandez. 1988. The dissociation of hydrogen sulfide in seawater. Limnol. Oceanogr. **33**: 269–274.

Moore, W. S., J. L. Sarmiento, and R. M. Key. 2008. Submarine groundwater discharge revealed by ^{228}Ra distribution in the upper Atlantic Ocean. Nat. Geosci. **1**: 309–311. doi:10.1038/ngeo183

Moore, W. S. 2010. The effect of submarine groundwater discharge on the ocean. Annu. Rev. Mar. Sci. **2**: 59–88. doi:10.1146/annurev-marine-120308-081019

Murphy, S. A., B. M. Solomon, S. Meng, J. M. Copeland, T. J. Shaw, and J. L. Ferry. 2014. Geochemical production of reactive oxygen species from biogeochemically reduced Fe. Environ. Sci. Technol. **48**: 3815–3821. doi:10.1021/es4051764

Neubauer, S. C., D. Emerson, and J. P. Megonigal. 2002. Life at the energetic edge: Kinetics of circumneutral iron oxidation by lithotrophic iron-oxidizing bacteria isolated from the wetland-plant rhizosphere. Appl. Environ. Microbiol. **68**: 3988–3995. doi:10.1128/AEM.68.8.3988-3995.2002

Omoregie, E. O., V. Mastalerz, G. de Lange, K. L. Straub, A. Kappler, H. Røy, A. Stadnitskaia, J.-P. Foucher, et al. 2008. Biogeochemistry and community composition of iron- and sulfur-precipitating microbial mats at the Chefren Mud Volcano (Nile Deep Sea Fan, Eastern Mediterranean). Appl. Environ. Microbiol. **74**: 3198–3215. doi:10.1128/AEM.01751-07

Quast, C., E. Pruesse, P. Yilmaz, J. Gerken, T. Schweer, P. Yarza, J. Peplies, and F. O. Glöckner. 2013. The SILVA ribosomal RNA gene database project: Improved data processing and web-based tools. Nucleic Acids Res. **41**: D590–D596. doi:10.1093/nar/gks1219

Rentz, J. A., C. Kraiya, G. W. Luther, III, and D. Emerson. 2007. Control of ferrous iron oxidation within circumneutral microbial iron mats by cellular activity and autocatalysis. Environ. Sci. Technol. **41**: 6084–6089. doi:10.1021/es062203e

Robinson, C., B. Gibbes, and L. Li. 2006. Driving mechanisms for groundwater flow and salt transport in a subterranean estuary. Geophys. Res. Lett. **33**: L03402. doi:10.1029/2005GL025247

Roden, E. E., D. Sobolev, B. Glazer, and G. W. Luther, III. 2004. Potential for microscale bacterial Fe redox cycling at the aerobic-anaerobic interface. Geomicrobiol. J. **21**: 379–391. doi:10.1080/01490450490485872

Rouxel, O., E. Sholkovitz, M. Charette, and K. J. Edwards. 2008. Iron isotope fractionation in subterranean estuaries. Geochim. Cosmochim. Acta **72**: 3413–3430. doi:10.1016/j.gca.2008.05.001

Roy, M., J. B. Martin, J. Cherrier, J. E. Cable, and C. G. Smith. 2010. Influence of sea level rise on iron diagenesis in an east Florida subterranean estuary. Geochim. Cosmochim. Acta **74**: 5560–5573. doi:10.1016/j.gca.2010.07.007

Roy, M., J. B. Martin, C. G. Smith, and J. E. Cable. 2011. Reactive-transport modeling of iron diagenesis and associated organic carbon remineralization in a Florida (USA) subterranean estuary. Earth Planet. Sci. Lett. **304**: 191–201. doi:10.1016/j.epsl.2011.02.002

Roy, M., J. B. Martin, J. E. Cable, and C. G. Smith. 2013. Variations of iron flux and organic carbon remineralization in a subterranean estuary caused by inter-annual variations in recharge. Geochim. Cosmochim. Acta **103**: 301–315. doi:10.1016/j.gca.2012.10.055

Russell, T. L., K. M. Yamahara, and A. B. Boehm. 2012. Mobilization and transport of naturally occurring enterococci

in beach sands subject to transient infiltration of seawater. Environ. Sci. Technol. **46**: 5988–5996. doi:10.1021/es300408z

Sáenz, J. P., E. C. Hopmans, D. Rogers, P. B. Henderson, M. A. Charette, S. Schouten, K. L. Casciotti, J. S. Sinninghe Damsté, et al. 2012. Distribution of anaerobic ammonia-oxidizing bacteria in a subterranean estuary. Mar. Chem. **136–137**: 7–13. doi:10.1016/j.marchem.2012.04.004

Santoro, A. E., A. B. Boehm, and C. A. Francis. 2006. Denitrifier community composition along a nitrate and salinity gradient in a coastal aquifer. Appl. Environ. Microbiol. **72**: 2102. doi:10.1128/AEM.72.3.2102-2109.2006

Santoro, A. E., C. A. Francis, N. R. de Sieyes, and A. B. Boehm. 2008. Shifts in the relative abundance of ammonia-oxidizing bacteria and archaea across physicochemical gradients in a subterranean estuary. Environ. Microbiol. **10**: 1068–1079. doi:10.1111/j.1462-2920.2007.01547.x

Slomp, C. P., and P. Van Cappellen. 2004. Nutrient inputs to the coastal ocean through submarine groundwater discharge: Controls and potential impact. J. Hydrol. (Amst) **295**: 64–86. doi:10.1016/j.jhydrol.2004.02.018

Smetacek, V., C. Klaas, V. H. Strass, P. Assmy, M. Montresor, B. Cisewski, N. Savoye, A. Webb, et al. 2012. Deep carbon export from a Southern Ocean iron-fertilized diatom bloom. Nature **487**: 313–319. doi:10.1038/nature11229

Søgaard, E. G., R. Aruna, J. Abraham-Peskir, and C. B. Koch. 2001. Conditions for biological precipitation of iron by *Gallionella ferruginea* in a slightly polluted ground water. Appl. Geochem. **16**: 1129–1137. doi:10.1016/S0883-2927(01)00014-2

Sorokin, D. Y., T. P. Tourova, E. M. Spiridonova, F. A. Rainey, and G. Muyzer. 2005. *Thioclava pacifica* gen. nov., sp. nov., a novel facultatively autotrophic, marine, sulfur-oxidizing bacterium from a near-shore sulfidic hydrothermal area. Int. J. Syst. Evol. Microbiol. **55**: 1069–1075. doi:10.1099/ijs.0.63415-0

Spiteri, C., P. Regnier, C. P. Slomp, and M. A. Charette. 2006. pH-dependent iron oxide precipitation in a subterranean estuary. J. Geochem. Explor. **88**: 399–403. doi:10.1016/j.gexplo.2005.08.084

Ullman, W. J., B. Chang, D. C. Miller, and J. A. Madsen. 2003. Groundwater mixing, nutrient diagenesis, and discharges across a sandy beachface, Cape Henlopen, Delaware (USA). Estuar. Coast. Shelf Sci. **57**: 539–552. doi:10.1016/S0272-7714(02)00398-0

Weiss, J. V., J. A. Rentz, T. Plaia, S. C. Neubauer, M. Merrill-Floyd, T. Lilburn, C. Bradburne, J. P. Megonigal, et al. 2007. Characterization of neutrophilic Fe(II)-oxidizing bacteria isolated from the rhizosphere of wetland plants and description of *Ferritrophicum radicicola* gen. nov. sp. nov., and *Sideroxydans paludicola* sp. nov. Geomicrobiol. J. **24**: 559–570. doi:10.1080/01490450701670152

Windom, H. L., W. S. Moore, L. F. H. Niencheski, and R. A. Jahnke. 2006. Submarine groundwater discharge: A large, previously unrecognized source of dissolved iron to the South Atlantic Ocean. Mar. Chem. **102**: 252–266. doi:10.1016/j.marchem.2006.06.016

Acknowledgments

Thanks to S. Krepski, S. Cone, K. Siegel, and C.C.'s geomicrobiology class, who assisted with sampling. C. Russoniello, M. Yao, D. Hubacz, C. Marnocha, E. Field, and S. Kato are acknowledged for their comments on drafts of this paper. This research was supported by National Science Foundation (NSF) grants Ocean Sciences (OCE)-1155290 (to C.C.), Earth Sciences (EAR)-1151682 (to C.C.), and EAR-1246554 (to H.M.), National Aeronautics and Space Administration (NASA) grant NNX12AG20G (to C.C. and G.L.), and Delaware Experimental Program to Stimulate Competitive Research (EPSCoR) with funds from NSF EPS-0814251 and the State of Delaware (to C.C. and H.M.).

Submitted 13 June 2014
Revised 13 November 2014
Accepted 13 November 2014

Associate editor: Ronnie Nøhr Glud